

Alma Mater Studiorum Università di Bologna
Archivio istituzionale della ricerca

Water-soluble silicon nanocrystals as NIR luminescent probes for time-gated biomedical imaging

This is the final peer-reviewed author's accepted manuscript (postprint) of the following publication:

Published Version:

Romano F., Angeloni S., Morselli G., Mazzaro R., Morandi V., Shell J.R., et al. (2020). Water-soluble silicon nanocrystals as NIR luminescent probes for time-gated biomedical imaging. *NANOSCALE*, 12(14), 7921-7926 [10.1039/d0nr00814a].

Availability:

This version is available at: <https://hdl.handle.net/11585/786143> since: 2020-12-31

Published:

DOI: <http://doi.org/10.1039/d0nr00814a>

Terms of use:

Some rights reserved. The terms and conditions for the reuse of this version of the manuscript are specified in the publishing policy. For all terms of use and more information see the publisher's website.

This item was downloaded from IRIS Università di Bologna (<https://cris.unibo.it/>).
When citing, please refer to the published version.

(Article begins on next page)

This is the final peer-reviewed accepted manuscript of:

Water-soluble silicon nanocrystals as NIR luminescent probes for time-gated biomedical imaging

F. Romano, S. Angeloni, G. Morselli, R. Mazzaro, V. Morandi, J. R. Shell, X. Cao, B. W. Pogue, P. Ceroni

Nanoscale 2020, 12, 7921–7926

The final published version is available online at:
<https://pubs.rsc.org/en/content/articlelanding/2020/nr/d0nr00814a>

Terms of use:

Some rights reserved. The terms and conditions for the reuse of this version of the manuscript are specified in the publishing policy. For all terms of use and more information see the publisher's website.

Water-soluble silicon nanocrystals as NIR luminescent probes for time-gated biomedical imaging

Francesco Romano,^a Sara Angeloni,^a Giacomo Morselli,^a Raffaello Mazzaro,^{a,b} Vittorio Morandi,^b Jennifer R. Shell,^c Xu Cao,^c Brian Pogue,^{c*} Paola Ceroni^{a*}

Luminescent probes based on silicon nanocrystals (SiNCs) have many advantages for bioimaging compared to more conventional quantum dots: abundance of silicon combined with its biocompatibility; tunability of SiNCs emission color in the red and NIR spectral region to gain deeper tissue penetration; long emission lifetimes of SiNCs (hundreds of μ s) enabling time-gated acquisitions to avoid background noise caused by tissue autofluorescence and scattered excitation light. Here we report a new three-step synthesis, based on low temperature thiol-ene click reaction that can afford SiNCs, colloiddally stable in water, with preserved bright red and NIR photoluminescence (band maximum at 735 and 945 nm for nanocrystals with diameter of 4 and 5 nm, respectively) and long emission lifetimes. Their luminescence is insensitive to dioxygen and sensitive to pH changes in the physiological range, enabling pH sensing. *In vivo* studies demonstrated tumor accumulation, 48 hours clearance and a 3-fold improvement of signal-to-noise ratio compared to steady-state imaging.

Introduction

Silicon nanocrystals (SiNCs) are an emerging class of luminescent quantum dots,^{1–7} featuring advantages in terms of high natural abundance of silicon, lack of biological toxicity compared to heavy metal-based nanoparticles,^{8,9} robustness of the surface passivating layer and bright long-lived (tens-to-hundreds of microseconds) luminescence. The main challenge to be addressed for biological applications of SiNCs is the coupling of bright long-lived luminescence with colloidal stability in water: aqueous environment facilitates (photo)oxidation of SiNC surface that brings about emission quenching. Until the current study, the main approaches reported to make water dispersible SiNCs are: (i) encapsulation within a water-soluble carrier, such as amphiphilic polymers,¹⁰ solid lipid nanoparticles¹¹ and micelles or liposomes,^{12–17} (ii) direct grafting of water solubilising polymers at SiNC surface, such as polyethylene glycol,^{18–20} poly(acrylic acid),^{21,22} (iii) surface functionalisation with highly polar moieties, such as carboxylic acids^{23–25} and ammonium groups,²⁶ or biomolecules.^{27–29} Most of these approaches suffer from formation of nano-aggregates containing multiple SiNCs and poor luminescence properties compared to SiNCs dispersed in organic solvents.

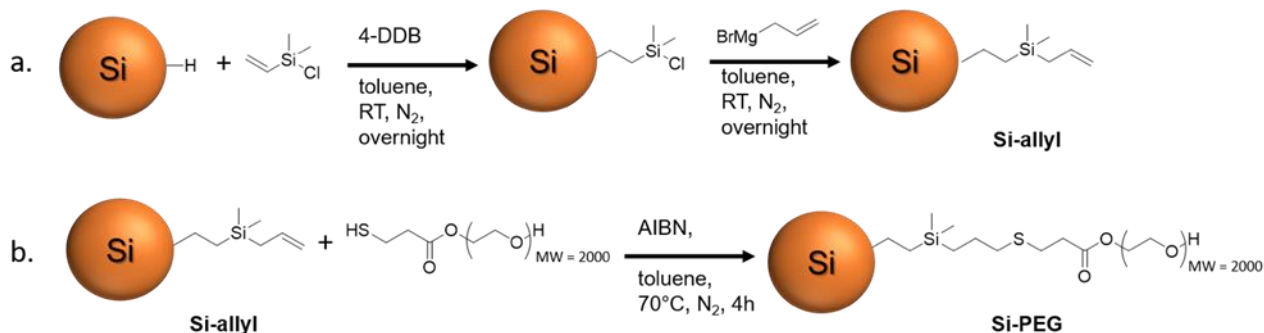
Here we describe a three-step synthetic protocol involving a thiol-ene click reaction,^{30,31} yielding SiNCs covalently functionalised only with PEG chains. This pegylated protective shell provides colloidal stability in water and protects SiNCs from interactions with serum proteins, like albumin, while keeping bright luminescence. The novelty and advantages of the presented synthetic approach are the following: (i) it can be applied to SiNCs of different size, e.g., average core diameter of 4 or 5 nm; (ii) the reaction procedure occurs at low temperature ($T \leq 70^\circ\text{C}$); (iii) a low amount of PEG derivative is required in the last functionalisation step, compared to the usual quantity employed in hydrosilylation reactions; (iv) the resulting SiNCs are colloiddally stable in water, not affected by surface photooxidation and display bright long-lived luminescence, insensitive to dioxygen and solvent quenching. The obtained SiNCs

exhibit unique optical properties compared to molecular fluorophores: (i) emission energy tuneable to the red and NIR spectral region, compatible with the biological window; (ii) high photoluminescence quantum yield; (iii) no sensitivity to molecular oxygen; (iv) long-lived luminescence decay in the hundreds of μ s, enabling time-gated detection (*vide infra*). Therefore, they are ideal candidates as luminescent probes for biomedical imaging.

Luminescence (usually fluorescence) imaging is an emerging technique in biomedicine.^{32–35} It is a niche compared to tomographic techniques (CT, MRI, PET), which rely on deep penetrating radiation and are widely employed in clinical practice today. However, fluorescence imaging offers advantages in terms of high temporal (real-time) acquisition and use of non-hazardous optical excitation. The main drawback is the limits of penetration depth: it is impossible to image through more than a few centimetres of tissue, so that optical imaging will never replace diagnostic radiology techniques in the human body, but it can be used for guiding surgery:^{36–39} For example, it is widely used in assessment of vascular flow in grafted tissues, tumour localisation (usually in skin, head, neck or breast cancer), sentinel-lymph node removal.

Currently, a lot of work is devoted towards NIR luminescence imaging because of reduced scattering of excitation light, minimal absorption and negligible autofluorescence by tissues, affording a higher signal to noise ratio and contrast. In particular, NIR-II chromophores^{32,40,41} and lanthanide nanoparticles^{42–44} with absorption and emission in the so-called NIR-II spectral region (usually defined as 1000–1700 nm) are gaining wider use to increase image resolution and contrast.

Time-gated detection coupled to NIR emission represents a further improvement in terms of signal-to-noise ratio and image contrast. The utilization of time-gated luminescence, in which luminescence is



Scheme 1 - Synthetic procedure for the functionalization of hydride-terminated SiNCs by allyl groups (a, **Si-allyl**) and post-functionalization via thiol-ene click reaction by PEG groups (b, **Si-PEG**).

recorded with a certain delay after excitation, suppresses scattered excitation light and short-lived autofluorescence of the sample. Until now, lanthanide metal complexes, upconverting nanoparticles^{45–47} and heavy-metal complexes, such as Pt or Pd have mostly been employed for this application with μ s-gating window, a time scale that allows easy implementation and low cost of the equipment.^{48–51}

SiNCs were already employed in luminescence imaging, for example in sentinel lymph node mapping,¹² but time-gated detection has not been explored. Time-gated luminescence was reported for a different silicon-based material, namely porous silicon nanoparticles, to image cells, organs or zebrafish.^{52–54} However, the dimension of the silicon core was much larger (>100 nm), the emission quantum yield was significantly lower (ca. 5%), sensitive to dioxygen quenching and limited to the visible region (red emission).

In the present paper, we demonstrate, for the first time, that SiNCs are viable alternatives for in vivo time-gated luminescence imaging in the NIR spectral window.

Results and discussion

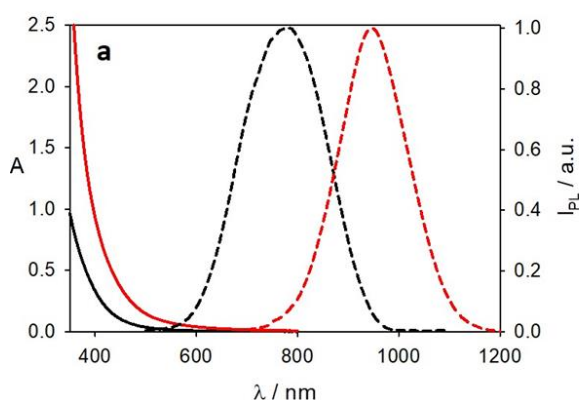
Synthesis

Hydride-terminated silicon nanocrystals with average diameter of 4 nm and 5 nm were prepared by thermal disproportionation of hydrogen silsesquioxane (HSQ) according to literature procedures.⁵⁵ The surface functionalization was performed by a three-step process (Scheme 1) in order to protect the SiNCs surface before PEG linkage

tetrafluoroborate (4-DDB), as radical initiator,^{56,57} (ii) Grignard nucleophilic addition to obtain the allyl-terminated SiNCs (**Si-allyl** in Scheme 1a) and (iii) thiol-ene click reaction with a previously prepared thiol-PEG derivative to yield water dispersible nanocrystals coated by PEG groups (**Si-PEG**, Scheme 1b). Silicon nanocrystals were characterized by NMR spectroscopy (Figure S1). The size distribution was evaluated by TEM analysis (Figure S2a) and is compatible with the corresponding dodecyl-terminated sample (Figure S2b) and previously reported samples of alkyl-terminated SiNCs prepared by the same methodology^{57–59}.

Photophysical properties

The absorption spectra of **Si-PEG** exhibit an unstructured absorption profile that is characteristic of Si nanocrystals (solid lines in Figure 1a).^{5,60} The photophysical data reported in Table 1 for **Si-allyl** and **Si-PEG** in toluene demonstrate that the radiative transition is characterized by the same energy, similar photoluminescence intensity decays (τ) and a decrease of the photoluminescence quantum yield (PLQY) in the case of 4-nm SiNCs. This decrease of PLQY with no effect on the lifetime might be indicative of the complete quenching of part of the nanocrystal ensemble (corresponding to lifetimes shorter than 5 μ s). This effect can be ascribed to partial surface oxidation during the click reaction of the fraction of nanocrystals with incomplete surface functionalization in step a (Scheme 1), as previously reported by some of us in a different post-functionalisation reaction of SiNCs.⁶¹



and maintain their good luminescent properties: (i) hydrosilylation at room temperature of hydride-terminated SiNCs in the presence of dimethylvinylchlorosilane and 4-decylbenzene diazonium

Figure 1 - (a) Absorption (solid lines) and normalized photoluminescence spectra (dashed lines) of **Si-PEG** nanocrystals in water with an average diameter of the silicon core of 4 nm (black-line) and 5 nm (red-line); (b) Picture of **Si-PEG** with a silicon core diameter of 4 nm dispersed in water under visible light, on the left, and under 365 nm UV light, on the right.

Table 1 - Photoluminescence band maximum (λ_{\max}), quantum yield (PLQY) and lifetime (τ) of **Si-PEG** and **Si-allyl** in toluene or distilled water. The reported diameters are referred to the silicon core.

		diameter = 4 nm			diameter = 5 nm		
		λ_{\max} (nm)	PLQY	τ (μ s)	λ_{\max} (nm)	PLQY	τ (μ s)
Si-allyl	toluene	770	0.41	74	955	0.30	135
Si-PEG	toluene	770	0.20	68	950	0.29	130
Si-PEG	water	735	0.16	60	945	0.18	120

The photophysical properties of **Si-PEG** in distilled water are reported in Figure 1 and Table 1: bright red to NIR emission (λ_{\max} =735 and 945 nm) are observed for average core diameter of 4 and 5 nm, respectively.

Stability and pH-sensitivity

Dynamic light scattering analysis (DLS) was used to evaluate hydrodynamic volumes of **Si-PEG** in water and their stability as a function of time. The results indicate diameters of around (30 ± 10) nm for both 4 and 5 nm **Si-PEG** nanoparticles (Figure S3). No significant change was observed over a one-week time interval, demonstrating no aggregation. Even the optical properties do not change with time: the samples remained transparent for several months when stored at room temperature. Moreover, photoluminescence lifetime of an **Si-PEG** sample in distilled water shows no change (Figure S4a) in a 1-day range and in blood serum at 37°C (Figure S4b), suggesting that the PEG surface functionalization was able to prevent interaction with serum proteins.

The pH dependence on the optical properties is also a fundamental issue for luminescent probes: at basic pH (>8) a significant decrease of lifetime was observed and lifetime changes were not fully reversible upon acidification to the initial pH value (Figure S5). On the contrary, at acidic pH, we observed a significant and fully reversible increase of lifetime (Figure 2), suggesting the possibility of implementing a pH sensor based on the luminescent lifetime of **Si-PEG**.

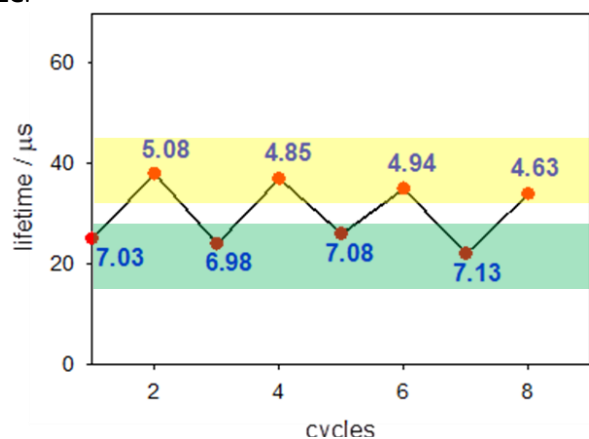


Figure 3 - Luminescence lifetimes as a function of pH (values reported in blue) in successive additions of HCl and KOH to a 7.5×10^{-7} M solution of 4 nm **Si-PEG** in water. λ_{ex} =365nm; λ_{em} > 550nm.

It is worth noting that the lifetimes reported in Figure 2 are lower than the value reported in distilled water (Table 1) and is due to the effect of ionic strength in aqueous solution. In addition, the

photoluminescence lifetime was proven not to be affected by the oxygen concentration (Figure S6), whose presence may affect the signal detected and reduce the reliability of the sensor.

Biodistribution and luminescence bioimaging

For the evaluation of biodistribution and potential of **Si-PEG** to be utilized for luminescence guided surgery, we selected an **Si-PEG** sample with average diameter of 4 nm because of the higher sensitivity of detectors in this spectral range as compared to the NIR-II spectral region. We found that *in vivo* (IV) injected **Si-PEG** were primarily excreted through the liver in athymic nude mice (Figure 3), with maximum excretion occurring at 24 h, as determined via *ex vivo* imaging.

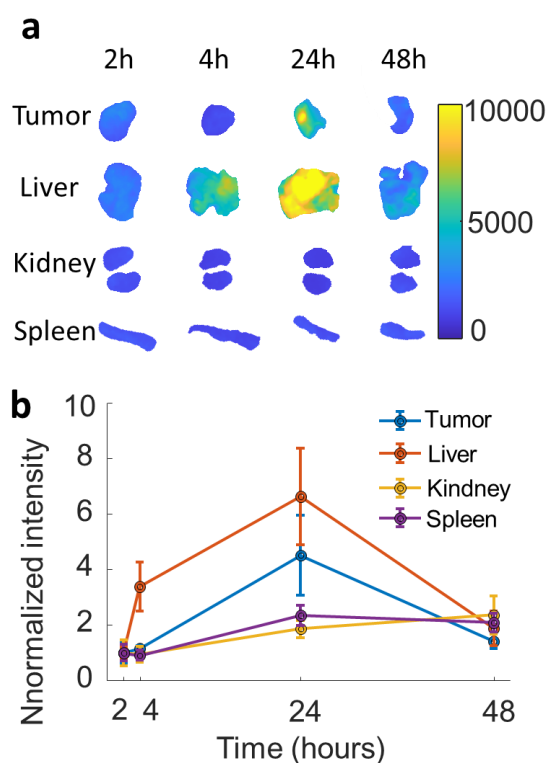


Figure 2 - Biodistribution of **Si-PEG** measured *ex-vivo* after *in vivo* injection. (a) Luminescence images of tumor, liver, kidney and spleen at different time points. (b) Normalised luminescence intensities as a function of time. The intensity value and error bar for each organ are the average and standard deviation of luminescence intensities of all pixels in the organ area.

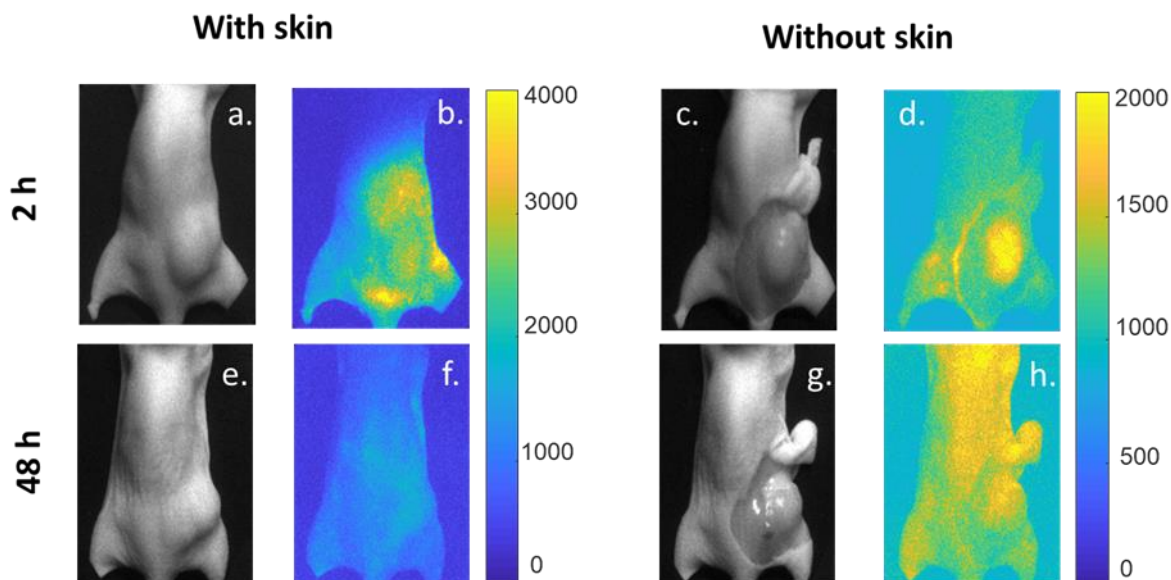


Figure 4 - SiNCs localize in MDA-MB-231 tumors. **Si-PEG** ($1.5 \mu\text{M}$) were IV injected and the luminescence in MDA-MB-231 tumors were imaged. (a and c) White light images with skin intact and with skin removed, respectively, 2 h post injection; (b and d) luminescence images 2 h post injection with skin intact and skin removed, respectively; (e and g) white light images with skin intact and skin removed, respectively, 48 h after injection; (f and h) luminescence images 48 h post injection.

In addition, a time study of accumulation of IV injected **Si-PEG** in mice with MDA-MB-231 flank tumors was conducted. **Si-PEG** were found to accumulate in these tumors over time, with maximum localization at 24 h. These SiNCs were found to remain in these tumors for 48 h (Figure 4). Therefore, SiNCs accumulated in the liver as well as in MDA-MB-231 tumors. Therefore, SiNCs accumulated in the liver as well as in MDA-MB-231 tumors. The efficiency of targeting the tumor in comparison to accumulation in the liver was estimated by the emission intensity ratio as a function of time: an

signal to background ratio is enhanced by a factor of 3 when utilizing time-gated luminescence imaging compared to steady-state luminescence imaging (Figure 5).

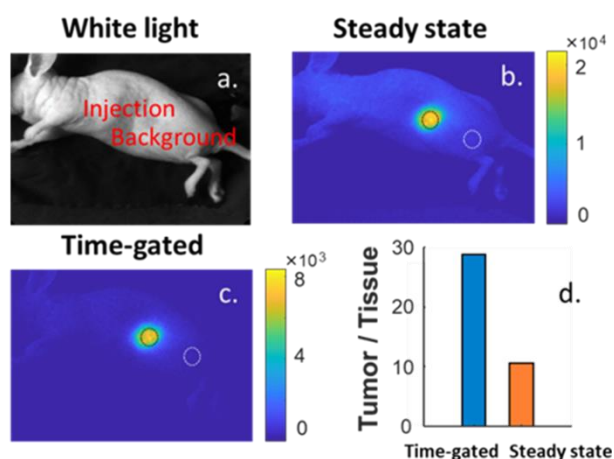
Conclusions

The current study demonstrates a new synthesis of polyethylene glycol functionalized silicon nanocrystals (average core diameter of 4 and 5 nm) with advantageous optical properties of NIR emission. It has also been shown that these nanoparticles have the potential to be utilized for luminescence guided surgery, since they accumulate in the tumor and are excreted within 48 hours, as demonstrated in mice with MDA-MB-231 tumors. In addition, due to the long emission lifetime of these SiNCs ($60 \mu\text{s}$), the signal to background ratio and background ambient light suppression can be enhanced via time-gated luminescence imaging.

Future studies are aimed at increasing the molar absorption coefficient of SiNCs in the red and NIR spectral region by a light-harvesting approach. This approach was already demonstrated in organic solvents:^{60–63} upon excitation of dye molecules appended at the nanocrystal surface, sensitized emission of the Si core is observed. This will enable red excitation of SiNCs coupled to time-gated NIR luminescence for deeper tissue penetration. Furthermore, conjugation of the terminal OH group of the PEG shell to a tumor targeting agent will be investigated for active targeting of the tumor.

Conflicts of interest

There are no conflicts to declare.



intensity ratio of 0.9 (tumor to liver) was observed at 2 h post

Figure 5 - Advantages of time-gated imaging. **Si-PEG** ($1.5 \mu\text{M}$) were subcutaneously injected into athymic nude mice (a) white light image indicating location of injection and location of quantitation of background luminescence; (b) steady state fluorescence imaging of SiNCs; (c) time-gated luminescence imaging; (d) difference in signal to background ratio afforded by time-gated imaging (delay $10 \mu\text{s}$).

injection (Figure S9).

A comparison of steady-state versus time-gated luminescence imaging was undertaken. **Si-PEG** ($1.5 \mu\text{M}$) were subcutaneously injected in athymic nude mice and the luminescence measured via both steady-state and time-gated detection. We found that the

Acknowledgements

The University of Bologna is gratefully acknowledged for financial support. R.M. gratefully acknowledges the European Union's Horizon 2020 research and innovation programme under GrapheneCore2 785219 – Graphene Flagship for partial funding. Work at Dartmouth was funded by National Institutes of Health grant R01 EB024498.

Ethical statement

This study was performed in strict accordance with the NIH guidelines for the care and use of laboratory animals (NIH Publication No. 85-23 Rev. 1985) and was approved by the Dartmouth Institutional Animal Care and Use Committee.

Notes and references

- 1 B. F. P. Mcvey and R. D. Tilley, *Acc. Chem. Res*, 2014, **47**, 3045–3051.
- 2 M. L. Mastronardi, E. J. Henderson, D. P. Puzzo and G. A. Ozin, *Adv. Mater.*, 2012, **24**, 5890–5898.
- 3 M. Dasog, J. Kehrle, B. Rieger and J. G. C. Veinot, *Angew. Chemie Int. Ed.*, 2016, **55**, 2322–2339.
- 4 R. J. Clark, M. Aghajamali, C. M. Gonzalez, L. Hadidi, M. A. Islam, M. Javadi, H. Mobarok, T. K. Purkait, C. J. T. Robidillo, R. Sinelnikov, A. N. Thiessen, J. Washington, H. Yu and J. G. C. Veinot, *Chem Mater*, 2017, **29**, 80–89.
- 5 R. Mazzaro, F. Romano and P. Ceroni, *Phys. Chem. Chem. Phys.*, 2017, **19**, 26507–26526.
- 6 X. Cheng, S. B. Lowe, P. J. Reece and J. J. Gooding, *Chem. Soc. Rev.*, 2014, **43**, 2680–2700.
- 7 M. Montalti, a. Cantelli and G. Battistelli, *Chem. Soc. Rev.*, 2015, **44**, 4853–4887.
- 8 O. Bondarenko, K. Juganson, A. Ivask, K. Kasemets, M. Mortimer and A. Kahru, *Arch. Toxicol.*, 2013, **87**, 1181–1200.
- 9 Z. Yang, Z. W. Liu, R. P. Allaker, P. Reip, J. Oxford, Z. Ahmad and G. Reng, *Nanotechnology, Brain, Futur.*, 2013, 313–332.
- 10 C. M. Hessel, M. R. Rasch, J. L. Hueso, B. W. Goodfellow, V. A. Akhavan, P. Puvanakrishnan, J. W. Tunnel and B. A. Korgel, *Small*, 2010, **6**, 2026–2034.
- 11 E. J. Henderson, A. J. Shuhendler, P. Prasad, V. Baumann, F. Maier-Flaig, D. O. Faulkner, U. Lemmer, X. Y. Wu and G. A. Ozin, *Small*, 2011, **7**, 2507–16.
- 12 F. Erogbogbo, K.-T. Yong, I. Roy, R. Hu, W.-C. Law, W. Zhao, H. Ding, F. Wu, R. Kumar, M. T. Swihart and P. N. Prasad, *ACS Nano*, 2011, **5**, 413–423.
- 13 X. Pi, T. Yu and D. Yang, *Part. Part. Syst. Charact.*, 2014, **31**, 751–756.
- 14 A. Elbaradei, S. L. Brown, J. B. Miller, S. May and E. K. Hobbie, *Phys. Rev. E*, 2016, **94**, 042804-1–9.
- 15 D. A. Silbaugh, L. Ferrer-Tasies, J. Faraudo, J. Veciana, N. Ventosa and B. A. Korgel, *Langmuir*, 2017, **33**, 14366–14377.
- 16 F. Erogbogbo, K. Yong, I. Roy, G. Xu, P. N. Prasad and M. T. Swihart, *ACS Nano*, 2008, **2**, 873–878.
- 17 B. J. Furey, D. A. Silbaugh, Y. Yu, A. C. Guillaussier, A. D. Estrada, C. Stevens, J. A. Maynard, B. A. Korgel and M. C. Downer, *Phys. Status Solidi Basic Res.*, 2018, **255**, 1–7.
- 18 V. Maurice, C. Slostowski, N. Herlin-Boime and G. Carrot, *Macromol. Chem. Phys.*, 2012, **213**, 2498–2503.
- 19 L. Ruizendaal, S. P. Pujari, V. Gevaerts, J. M. J. Paulusse and H. Zuilhof, *Chem. - An Asian J.*, 2011, **6**, 2776–2786.
- 20 M. A. Islam, R. Sinelnikov, M. A. Howlader, A. Faramus and J. G. C. Veinot, *Chem. Mater.*, 2018, **30**, 8925–8931.
- 21 Y. He, Z.-H. H. Kang, Q.-S. S. Li, C. H. A. Tsang, C.-H. H. Fan and S.-T. T. Lee, *Angew. Chemie - Int. Ed.*, 2009, **48**, 128–132.
- 22 Z. F. Li and E. Ruckenstein, *Nano Lett.*, 2004, **4**, 1463–1467.
- 23 R. J. Clark, M. K. M. Dang and J. G. C. Veinot, *Langmuir*, 2010, **26**, 15657–15664.
- 24 Y. He, Y. Zhong, F. Peng, X. Wei, Y. Su, Y. Lu, S. Su, W. Gu, L. Liao and S.-T. Lee, *J. Am. Chem. Soc.*, 2011, **133**, 14192–14195.
- 25 Y. Yu, C. M. Hessel, T. D. Bogart, M. G. Panthani, M. R. Rasch and B. A. Korgel, *Langmuir*, 2013, **29**, 1533–1540.
- 26 K. K. Chen, K. Liao, G. Casillas, Y. Li and G. A. Ozin, *Adv. Sci.*, 2016, **3**, 1500263.
- 27 F. Erogbogbo, C.-W. Chang, K.-T. Yong, M. T. Swihart and P. N. Prasad, *Bioconjugate Chem*, 2011, **22**, 1081–1088.
- 28 C. C. Tu, K. P. Chen, T. A. Yang, M. Y. Chou, L. Y. Lin and Y. K. Li, *ACS Appl. Mater. Interfaces*, 2016, **8**, 13714–13723.
- 29 Y. Zhai, M. Dasog, R. B. Snitynsky, T. K. Purkait, M. Aghajamali, A. H. Hahn, C. B. Sturdy, L. Lowary and J. G. C. Veinot, *J. Mater. Chem. B*, 2014, **2**, 8427–8433.
- 30 X. Cheng, R. Gondosiswanto, S. Ciampi, P. J. Reece and J. J. Gooding, *Chem Commun*, 2012, **48**, 11874–11876.
- 31 C. J. T. Robidillo, M. Aghajamali, A. Faramus, R. Sinelnikov and J. G. C. Veinot, *Nanoscale*, 2018, **10**, 18706–18719.
- 32 C. Li and Q. Wang, *ACS Nano*, 2018, **12**, 9654–9659.
- 33 Q. T. Nguyen, E. S. Olson, T. A. Aguilera, T. Jiang, M. Scadeng, L. G. Ellies and R. Y. Tsien, *Proc. Natl. Acad. Sci.*, 2010, **107**, 4317–4322.
- 34 R. Weissleder, *Nat. Biotechnol.*, 2001, **19**, 316–317.
- 35 M. Y. Berezin and S. Achilefu, *Chem Rev*, 2010, **110**, 2641–2684.
- 36 Q. T. Nguyen and R. Y. Tsien, *Nat. Rev. Cancer*, 2013, **13**, 653–662.
- 37 S. Gioux, H. S. Choi and J. V. Frangioni, *Mol. Imaging*, 2010, **9**, 237–255.
- 38 H. S. Choi and J. V. Frangioni, *Mol. Imaging*, 2010, **9**, 291–310.
- 39 A. V Dsouza, E. R. Henderson, K. S. Samkoe, B. W. Pogue, A. V Dsouza, H. Lin, E. R. Henderson, K. S. Samkoe and B. W. Pogue, *J. Biomed. Opt.*, 2016, **21**, 080901-1–15.
- 40 H. Guosong, L. A. Alexander and D. Hongjie, *Nat. Biomed. Eng.*, , DOI:10.1038/s41551-016-0010.
- 41 P. Liu, X. Mu, X. Zhang and D. Ming, ,

DOI:10.1021/acs.bioconjchem.9b00610.

- 42 Y. Zhong, Z. Ma, F. Wang, X. Wang, Y. Yang, Y. Liu, X. Zhao, J. Li, H. Du, M. Zhang, Q. Cui, S. Zhu, Q. Sun, H. Wan, Y. Tian, Q. Liu, W. Wang, K. C. Garcia and H. Dai, *Nat. Biotechnol.*, 2019, **37**, 1322–1331.
- 43 Y. Fan, P. Wang, Y. Lu, R. Wang, L. Zhou, X. Zheng, X. Li, J. A. Piper and F. Zhang, *Nat. Nanotechnol.*, 2018, **13**, 941–946.
- 44 H. Zhang, Y. Fan, P. Pei, C. Sun, L. Lu and F. Zhang, *Angew. Chemie - Int. Ed.*, 2019, **58**, 10153–10157.
- 45 E. J. New, D. Parker, D. G. Smith and J. W. Walton, *Curr. Opin. Chem. Biol.*, 2010, **14**, 238–246.
- 46 L. Sun, R. Wei, J. Feng and H. Zhang, *Coord. Chem. Rev.*, 2018, **364**, 10–32.
- 47 A. J. Amoroso and S. J. A. Pope, *Chem Soc Rev*, 2015, **44**, 4723–4742.
- 48 R. Yusuf, D. Co, W. Zaher, L. J. Mortensen, C. Alt, S. A. Vinogradov, D. T. Scadden and C. P. Lin, *Nature*, 2014, **508**, 269–273.
- 49 E. Baggeley, J. A. Weinstein and J. A. G. Williams, in *Luminescent and Photoactive Transition Metal Complexes as Biomolecular Probes and Cellular Reagents. Structure and Bonding*, vol 165, Springer, Berlin, Heidelberg, 2014.
- 50 K. Y. Zhang, Q. Yu, H. Wei, S. Liu, Q. Zhao and W. Huang, *Chem Rev*, 2018, **118**, 1770–1839.
- 51 T. Esipova, M. Barrett, E. Erlebach, A. Masunov, B. Weber and S. Vinogradov, *Cell Metab*, 2019, **29**, 736–744.
- 52 J. Joo, X. Liu, V. R. Kotamraju, E. Ruoslahti, Y. Nam and M. J. Sailor, *ACS Nano*, 2015, **9**, 6233–6241.
- 53 W. Yang, P. K. Srivastava, S. Han, L. Jing, C. Tu and S. Chen, *Anal. Chem.*, 2019, **91**, 5499–5503.
- 54 N. Ohta and Y. Li, *ACS Photonics*, 2017, **4**, 1306–1315.
- 55 C. M. Hessel, E. J. Henderson and J. G. C. Veinot, *Chem. Mater.*, 2006, **18**, 6139–6146.
- 56 I. M. D. Höhle, J. Kehrle, T. K. Purkait, J. G. C. Veinot and B. Rieger, *Nanoscale*, 2015, **7**, 914–918.
- 57 A. Arrigo, R. Mazzaro, F. Romano, G. Bergamini and P. Ceroni, *Chem. Mater.*, 2016, **28**, 6664–6671.
- 58 Y. Yu, G. Fan, A. Fermi, R. Mazzaro, V. Morandi, P. Ceroni, D.-M. Smilgies and B. A. Korgel, *J. Phys. Chem.*, 2017, **121**, 23240–23248.
- 59 J. A. Kelly and J. G. C. Veinot, *ACS Nano*, 2010, **4**, 4645–4656.
- 60 M. Locritani, Y. Yu, G. Bergamini, M. Baroncini, J. K. Molloy, B. A. Korgel and P. Ceroni, *J. Phys. Chem. Lett.*, 2014, **5**, 3325–3329.
- 61 L. Ravotto, Q. Chen, Y. Ma, S. A. Vinogradov, M. Locritani, G. Bergamini, F. Negri, Y. Yu, B. A. Korgel and P. Ceroni, *Chem*, 2017, **2**, 550–560.
- 62 F. Romano, Y. Yu, B. A. Korgel, G. Bergamini and P. Ceroni, *Top. Curr. Chem.*, 2016, **374**, 89–106.
- 63 R. Mazzaro, A. Gradone, S. Angeloni, G. Morselli, P. G. Cozzi, F. Romano, A. Vomiero and P. Ceroni, *ACS Photonics*, , DOI:10.1021/acsphotonics.9b00802.